Using urban climate modelling and improved land use classifications to support climate change adaptation in urban environments: A case study for the city of Klagenfurt, Austria

Article *in* Urban Climate · January 2020

DOI: 10.1016/j.uclim.2020.100582

CITATIONS
10

READS
304

9 authors, including:

Sandro M. Oswald
Central Institution of Meteorology and Geodynamics
19 PUBLICATIONS **49** CITATIONS
SEE PROFILE

Brigitta Hollosi
Central Institute for Meteorology and Geodynamics
17 PUBLICATIONS **111** CITATIONS
SEE PROFILE

Maja Zuvela-Aloise
Central Institute for Meteorology and Geodynamics
39 PUBLICATIONS **466** CITATIONS
SEE PROFILE

Linda M. See
International Institute for Applied Systems Analysis
348 PUBLICATIONS **11,637** CITATIONS
SEE PROFILE

Urban Climate 31 (2020) 100582

Contents lists available at ScienceDirect

Urban Climate

journal homepage: www.elsevier.com/locate/uclim

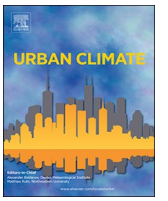

Using urban climate modelling and improved land use classifications to support climate change adaptation in urban environments: A case study for the city of Klagenfurt, Austria

Sandro M. Oswald[a,e,*], Brigitta Hollosi[a], Maja Žuvela-Aloise[a], Linda See[b], Stefan Guggenberger[c], Wolfgang Hafner[c], Gundula Prokop[d], Alexander Storch[d], Wolfgang Schieder[d]

[a] *Zentralanstalt für Meteorologie und Geodynamik (ZAMG), Vienna, Austria*
[b] *International Institute for Applied Systems Analysis (IIASA), Laxenburg, Austria*
[c] *International Project Management Agency Klagenfurt on Lake Wörthersee GmbH (IPAK), Klagenfurt, Austria*
[d] *Environment Agency (UBA), Vienna, Austria*
[e] *Institute of Meteorology, University of Natural Resources and Life Science (BOKU), Vienna, Austria*

ARTICLE INFO

Keywords:
Urban Heat Island
Climate adaptation measures
MUKLIMO_3
Green roofs

ABSTRACT

This study outlines the results of current and future climate scenarios, and potentially realizable climate adaptation measures, for the city of Klagenfurt, Austria. For this purpose, we used the microscale urban climate model (MUKLIMO_3), in conjunction with the cuboid method, to calculate climate indices such as the average number of summer and hot days per year. For the baseline simulation, we used meteorological measurements from 1981 to 2010 from the weather station located at Klagenfurt Airport. Individual building structures and canopy cover from several land monitoring services were used to derive accurate properties for land use classes in the study domain. To characterize the effectiveness of climate adaptation strategies, we compared changes in the climate indices for several (future) climate adaptation scenarios to the reference simulation. Specifically, we considered two major adaptation pathways: (i) an increase in the albedo values of sealed areas (i.e., roofs, walls and streets) and (ii) an increase in green surfaces (i.e., lawns on streets and at roof level) and high vegetated areas (i.e., trees). The results indicate that some climate adaptation measures show higher potential in mitigating hot days than others, varying between reductions of 2.3 to 11.0%. An overall combination of adaptation measures leads to a maximum reduction of up to 44.0%, indicating a clear potential for reduction/mitigation of urban heat loads. Furthermore, the results for the future scenarios reveal the possibility to remain at the current level of urban heat load during the daytime over the next three decades for the overall combination of measures.

Abbrevations: CORDEX, Coordinated Regional Downscaling Experiment; DWD, Deutscher Wetterdienst/German Meteorological Service; ETCCDI, Expert Team on Climate Change Detection and Indices; GCM, Global Climate Model; HD, Number of hot days; LISA, Land Information System Austria; LU, Land use; RCM, Regional Climate Model; RCP, Representative Concentration Pathways; SD, Number of summer days; TMC, Threshold method classification; UA, Urban Atlas; UHI, Urban Heat Island

* Corresponding author at: Zentralanstalt für Meteorologie und Geodynamik (ZAMG), Vienna, Austria.
E-mail address: sandro.oswald@zamg.ac.at (S.M. Oswald).

https://doi.org/10.1016/j.uclim.2020.100582
Received 30 July 2019; Received in revised form 19 December 2019; Accepted 1 January 2020

1. Introduction

Today around 55% of the world's population resides in urban environments, and the rate of city dwellers is projected to increase to 68% by 2050 (UN, 2018). The rising rates of urbanization have led to an increase in impervious areas that affect or modulate the local surface energy balance. As a result, urban areas are prone to higher ambient air temperatures than surrounding rural areas, a phenomenon commonly referred to as the Urban Heat Island (UHI) effect (Landsberg, 1981; Oke, 1982). The UHI effect scales with city size and is modulated by the ambient terrain and surface structure of the urban settlement (Arnfield, 2003; Zhou et al., 2017). Several studies have investigated UHIs in larger European cities (e.g., Dessai (2003) and more recently, D'Ippoliti et al. (2010) and Chrysanthou et al. (2014)). While much focus has been placed on megacities, smaller cities are also affected by the UHI. Therefore, local governments and urban planners need information about implementing measures to counteract (and mitigate) the thermal discomfort of their city's inhabitants. Future projections indicate substantial growth rates in urbanization (UN, 2018) and a continued (scenario-dependent) global warming (IPCC, 2013). Hence, urban heat loads and the related negative impacts of UHI effects are expected to intensify, which will lead to thermal discomfort and negatively impact the quality of life in urban areas (UN, 2019).

Thus, to combat the negative effects associated with the UHI, successful urban planning strategies are needed to mitigate the (excessive) increases in ambient air temperature T_a in urban areas and potentially even reduce future heat loads below present day levels (Taha et al., 1988; McPherson, 1994; Hassid et al., 2000; Orehounig et al., 2014). To achieve this goal, various climate adaptation measures including highly reflective surfaces to decrease surface temperatures (i.e., brightly colored, painted roofs and/or streets) (Taha, 1997; Bretz et al., 1998; Santamouris et al., 2011), or additional vegetated areas to enhance evapotranspiration (Gill et al., 2007; Alexandri and Jones, 2008; Qiu et al., 2013) are frequently considered in urban planning. A combination of a number of different climate adaptation measures as, for example, shown in Laukkonen et al. (2009), Voskamp and de Ven (2015) and Žuvela-Aloise et al. (2017), can increase resilience against (extreme) heat loads in urban areas.

Several studies are based on microscale urban climate models, but they simulate only part of a city or only a single street canyon for a short period of time, e.g. one to three months (see, for example, Müller et al. (2013)). Other works have simulated UHI patterns and heat wave days for whole cities as, e.g., Brussels, but they considered only a time period of ten or 20 years due to the large computational efforts required (Lauwaet et al., 2015; Lauwaet et al., 2016). However, future climate projections (and the large variability in meteorological conditions) must be considered over several decades (i.e., at least 30 years) to identify climate change signals. Here, we use climate indices such as the average number of summer days $\overline{SD}$ (days where maximum daily $T_a \geq 25$ °C) and hot days $\overline{HD}$ (days where maximum daily $T_a \geq 30$ °C) per year to identify the (sub)urban heat load distribution in the city as a whole, to evaluate as many adaptation measures as possible using accurate urban information received from local authorities and to simulate long term changes in climate conditions.

To determine the changes in urban heat load on longer timescales, simulations can be performed with several climate models. However, due to computational requirements, simplified modelling approaches are needed for practical applications. While some methods use combined dynamical and statistical approaches, like different weather pattern classifications (Hoffmann and Schlünzen, 2013), others use simplified urban physics considering seasonal UHI trends (UrbClim) (Ridder et al., 2015). Here, we use the microscale urban climate model MUKLIMO_3 (see Section 2.1), developed by the German Meteorological Service (DWD) (Sievers, 1995) and the so-called cuboid method (Früh et al., 2011). This combination of a dynamical and statistical approach allows analysis of a large ensemble of global/regional climate model results in a computationally efficient way in contrast to standard downscaling methods with a single model approach (Lauwaet et al., 2016; Gidhagen et al., 2020).

In order to analyze heat load changes on a longer timescale and to calculate averaged climate indices, we performed the simulations using information on current urban structures based on data from the local city government and different land monitoring services. The type and extent of adaptation measures analyzed in this study were chosen to represent realistic adjustments in urban environments relative to the current situation and include two sets of scenarios: (a) the increase in albedo values of (i) roofs, (ii) walls and (iii) streets/sidewalks; and (b) the increase in green spaces through (iv) low vegetated areas (ornamental lawns), (v) green roofs, and (vi) the number of trees within the urban area, (vii) a decrease in sealed areas, and (viii) afforestation near the city. These scenarios are either investigated as the implementation of individual measures or as the combination of several adaptation measures.

This study aims to evaluate the effectiveness of different climate adaptation measures to reduce urban heat loads during the daytime for the medium-sized city of Klagenfurt in the south of Austria. The city has a population of 100,993 (1 January, 2019) (Municipality of City of Klagenfurt, 2019b), and through immigration in recent years, Klagenfurt has experienced continuous urban growth (Municipality of City of Klagenfurt, 2019a). While tropical nights rarely occur in a city between the Alps like Klagenfurt (see Fig. S1 in the Supplementary Material), HD y^{-1} and the corresponding energy demand will become more and more important in the future (Isaac and Van Vuuren, 2009; van Ruijven et al., 2019). An evaluation of HD y^{-1} indicates a clear need to act against increasing heat loads in (sub)urban areas during the daytime (see Fig. 1).

This study focuses on two main aspects. The first is the simulation of $\overline{SD}$ y^{-1} (chosen based on the recommendations of the Expert Team on Climate Change Detection and Indices (ETCCDI) (Karl et al., 1999)) and $\overline{HD}$ y^{-1} (to characterize the most relevant factor of heat loads during the daytime) for the time periods 1971–2000 and 1981–2010, and under future climate projections for the time periods 2021–2050 and 2071–2100. The second aspect is the evaluation of the effectiveness of the eight aforementioned climate adaptation measures and their combination with respect to the difference in the climate indices compared to the reference simulation (1981–2010) and also with respect to future climate projections (2021–2050 and 2071–2100). In addition, individual simulations with hourly values of T_a (2 m above ground) are provided to illustrate the diurnal variability.

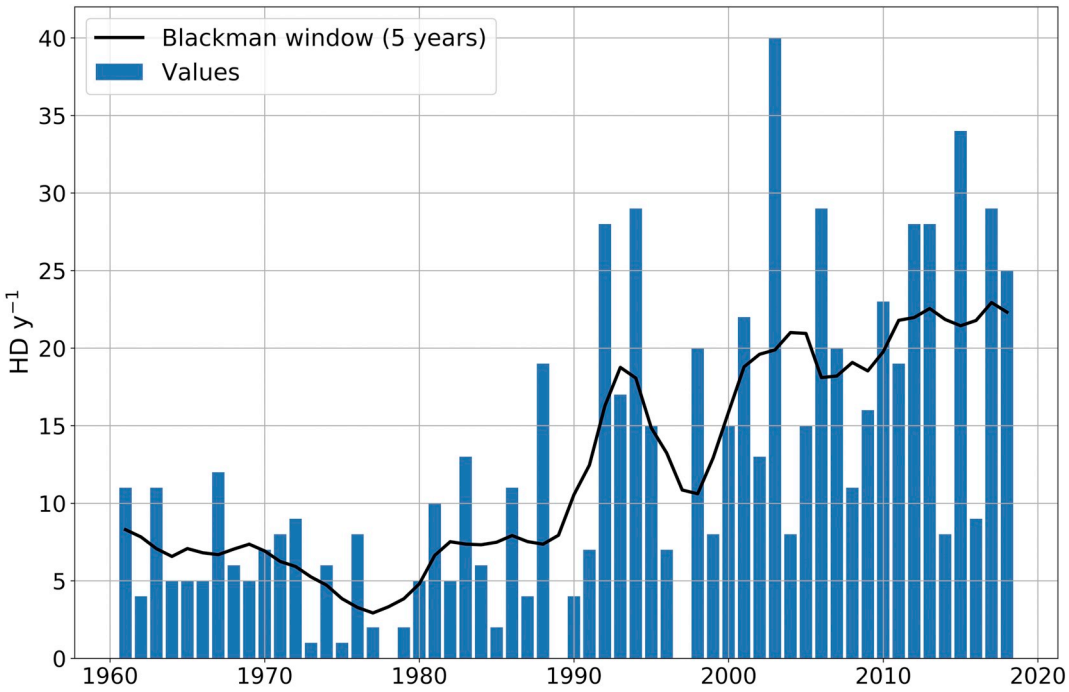

Fig. 1. Number of hot days per year (HD y^{-1} defined as the maximum daily ambient air temperature ≥ 30°C) measured at Klagenfurt Airport from 1961 to 2018. The black line shows a moving average smoothing with a Blackman filter (window size of five years).

2. Material and methods

2.1. Urban climate model

The urban climate model applied in this study is the microscale urban climate model MUKLIMO_3 (Sievers, 1995, 2012, 2016), which simulates atmospheric temperature, humidity and wind flow in urban areas on a three-dimensional grid. The latest thermodynamic version of MUKLIMO_3 (v141010 from 2014 used in this study) is based on the previous versions of the model with a generalized streamfunction-vorticity formulation (Sievers and Zdunkowski, 1986; Sievers, 1995) with additions of soil heat and moisture budgets (Sievers et al., 1983), a vegetation model (Siebert et al., 1992), parameterization of the atmospheric flow in the unresolved built-up environment following the approach of Gross (1989) and short-wave irradiance parametrization as described in Sievers and Früh (2012).

The individual climate indices were derived based on daily maximum temperature fields calculated with the MUKLIMO_3 model, which were combined with long-term climate information using the cuboid method approach (see Section S1 in the Supplementary Material for further explanation) (Früh et al., 2011; Žuvela-Aloise et al., 2014). To this end, idealized daily MUKLIMO_3 simulations were performed for eight different representative weather conditions under which excessive heat load in the urban area is expected to occur. Time-varying 1D vertical profiles of air temperature, relative humidity, wind speed and radiation have been used as meteorological inputs. Furthermore, the two dominant wind directions in the study domain were considered to account for the influence of the wind direction on the air temperature fields, which resulted in a total of 16 MUKLIMO_3 simulations.

The mean daily T_a, 2 m relative humidity and 10 m wind velocity, as well as hourly wind direction for 30-year periods were used to derive climate indices using a tri-linear interpolation between the 16 simulations as described in Früh et al. (2011), Žuvela-Aloise et al. (2014) and Geletic et al. (2019). For the historical climate analysis (1971–2010), this long-term observational time series were taken from the monitoring station outside the city, in this case Klagenfurt Airport (46° 39, 14° 20 at a sea level of 447 m) (ZAMG, 2019). Based on the measurements of the wind direction during 1971–2010, the two prevalent directions are 335° (NNW) and 125° (ESE). Finally, extracted time series of these meteorological parameters from regional climate models for different climate scenarios (i.e., with specific Representative Concentration Pathways (RCPs)) were taken as inputs to calculate the future climate projections at the urban scale (see Section 2.3).

In addition to the meteorological data, the MUKLIMO_3 model requires a digital elevation model and land use (LU) information as inputs. The LU types were split into four main categories: (i) buildings, (ii) trees, (iii) low vegetated areas, and (iv) water. Categories (i) to (iii) can include impervious areas (i.e., streets/sidewalks) and also unvegetated pervious areas. The percentage of each LU type per grid cell can be used to define and describe the properties of each LU class. The model domain covers the whole city of Klagenfurt and parts of the surrounding districts (see Fig. S3 in the Supplementary Material) with a domain size of 198 × 160 × 44 cells using a horizontal spatial resolution of 100 m.

Table 1
Characteristic parameters for building land use classes in Klagenfurt based on different land use classification approaches (Initial: Urban Atlas, Final: Threshold method) where f_b is the fraction of buildings, h_b is the average building height, f_p is the fraction of pavement and f_v is the fraction of the vegetation cover. Note that the remaining area fraction is unvegetated, pervious area, which sums to 1.

		Initial				Final			
Class	Description	f_b	h_b	f_p	f_v	f_b	h_b	f_p	f_v
1	Continuous (Cont.) UF[a]	0.45	17.0	0.41	0.10	0.41	14.0	0.39	0.17
2	Discont. dense UF	0.23	14.0	0.32	0.37	0.22	10.0	0.34	0.38
3	Discont. medium density UF	0.18	10.0	0.26	0.46	0.17	8.0	0.26	0.47
4	Discont. low density UF	0.14	12.0	0.19	0.56	0.14	9.0	0.23	0.54
5	Discont. very low density UF	0.11	8.0	0.14	0.61	0.09	9.0	0.20	0.58
7	Industrial and military units	0.22	7.0	0.40	0.33	0.11	6.0	0.30	0.54
12	Airport	0.03	8.0	0.21	0.75	0.02	8.0	0.17	0.80

[a] UF = urban fabric.

2.2. Land use, land cover and orography

The Copernicus Land Monitoring Service portal, initiated by the European Environment Agency, provides detailed land cover and LU information over major cities in the European Union in the form of the Urban Atlas (UA) (European Union, 2018). The UA is available for cities with a population larger than 100,000 inhabitants for 2006 and for cities with more than 50,000 inhabitants for 2012. Other high resolution layers available from Copernicus include the imperviousness layer and forest cover at a resolution of 20 m. In addition to these data sets, a detailed area zoning plan, including the heights of individual buildings, and a registry of public trees (with crown and stem heights) were made available by the local city government of Klagenfurt.

The LU classification of the UA (see Fig. S3a in the Supplementary Material) was combined with the information received from the local city government including the surrounding districts to evaluate the LU parameters statistically. These parameters were used to describe the initial urban properties for each LU class (see Tables 1 and 2 in columns 3 to 6, respectively). In addition, data from the Land Information System Austria (LISA), covering large parts of Austria with a 1 m resolution (GeoVille GmbH, 2016), were used. LISA provides detailed land cover data, which was generated from satellite images covering the period 2014 until 2016 and contains eleven different land cover classes, e.g., buildings, annual crops, cobbled pavements. Due to the high number of sub-classes, the data set was simplified into four main categories as required by MUKLIMO_3 plus two additional classes (impervious and pervious areas) (see Table S1 in the Supplementary Material).

The digital surface model from the International Project Management Agency Klagenfurt (IPAK) has been used as additional information. Taking the difference between the digital surface and digital elevation model and then combining this with LISA allowed us to calculate the precise position and height of each building and tree with a 1 m spatial resolution.

2.2.1. Threshold method

As detailed above, the land cover map provided by LISA was used to create a rasterized building height/position map for the study domain. These maps, combined with the calculated properties of each LU class, were used to define the threshold method classification (TMC) proposed here. This method determines the percentage of each main LU type (as defined by LISA), averages the building heights in each grid cell and reclassifies the current LU class of the UA with the values in Tables 1 and 2 (Initial) as thresholds. After using the TMC, zonal statistics were applied to each LU class to produce the final values for the MUKLIMO_3 model inputs (see Tables 1 and 2 in columns 7 to 10, respectively).

Table 2
Characteristic parameters for vegetated classes in Klagenfurt based on different land use classification approaches (Initial: Urban Atlas, Final: Threshold method) where h_t is the tree height, σ_t is the number of trees, f_v is the fraction of vegetation cover and f_p is the fraction of pavement. Note that the remaining area fraction is unvegetated, pervious area, which sums to 1. σ_t is independent of paved and unpaved surfaces.

		Initial				Final			
Class	Description	h_t	σ_t	f_v	f_p	h_t	σ_t	f_v	f_p
8	Transit roads and AL[a]	9.0	0.25	0.55	0.31	7.0	0.28	0.49	0.33
9	Other roads and AL	9.0	0.07	0.43	0.43	9.0	0.07	0.38	0.51
10	Railways and AL	10.0	0.06	0.21	0.62	9.0	0.09	0.24	0.54
16	Green urban areas	13.0	0.35	0.52	0.24	12.0	0.29	0.65	0.10
17	Sports and leisure facilities	15.0	0.21	0.64	0.18	16.0	0.23	0.65	0.16
23	Forest	16.0	0.81	0.90	0.01	17.0	0.78	0.88	0.01

[a] AL = associated land.

2.3. Future climate projections - EURO-CORDEX

The World Climate Research Programme initialized the Coordinated Regional Downscaling Experiment (CORDEX) with the vision to support, coordinate and improve regional climate scenarios with global partnerships (WCRP, 2019; Giorgi et al., 2006). For Europe, the EURO-CORDEX research project (Jacob et al., 2013) pooled future climate projections via Regional Climate Models (RCMs) at a 50 km and 12.5 km spatial resolution based on RCPs as defined in the Fifth Assessment Report of the Intergovernmental Panel on Climate Change (IPCC, 2013; Moss et al., 2010). These simulations provide information on essential meteorological parameters until 2100 under different climate change scenarios.

To estimate possible future urban climate scenarios from the EURO-CORDEX model database, we used model outputs from three different RCMs combined with six Global Climate Models (GCMs) at the 12.5 km spatial resolution (see Table S2 in the Supplementary Material) under RCP4.5 and RCP8.5 (IPCC, 2013) for two time periods 2021–2050 and 2071–2100. RCP4.5 corresponds to a scenario in which CO_2 emissions are set to peak by 2040 while RCP8.5 is a more extreme scenario in which CO_2 emissions will continue to rise until 2100. The data for the city of Klagenfurt and the immediate surroundings were selected from a model area of 3 × 3 grid cells, i.e., averaged values over 37.5 × 37.5 km^2. Daily outputs of mean T_a, relative humidity at a 2 m height, near-surface wind speed and wind direction were then extracted.

The values of wind speed and direction were taken from the grid cell closest to the actual height of Klagenfurt Airport. Furthermore, T_a was bias corrected using the measurements between 1971 and 2000 from the monitoring weather station, applying the quantile mapping method (qmap) package in R (Gudmundsson, 2016). This module uses non-parametric quantile mapping by estimating an empirical cumulative distribution function of observations and modeled values to derive their quantiles following the works of Boé et al. (2007) and Gudmundsson et al. (2012). Finally, the relative humidity was corrected by assuming that the initial absolute humidity of the EURO-CORDEX model output is true. With the transformed T_a, the relative humidity was recalculated.

2.4. Implementation of the climate adaptation measures

In order to quantify the maximum obtainable “cooling” effect inside urban areas, individual adaptation measures and their combination were analyzed. The physical properties of these measures are based on assumptions from evapotranspiration and energy balance models (Gross, 2012). The implementation in the model configuration was performed individually through the variation of different parameters defined for each LU class.

2.4.1. Highly reflective surfaces

Highly reflective surfaces, i.e., with enhanced albedo values, are used for sealed areas like roofs, walls and streets/sidewalks. The shortwave reflectivity of the roofs α_r (initially 0.2) and walls α_w (initially 0.3) was increased to 0.5, and the value of the streets α_{st} (initially 0.2) was set to 0.4 for the LU classes 1 to 7 (see Fig. 2). These LU classes represent the main urban building areas. Furthermore, the albedo values were chosen based on (fine) dust accumulation on roofs (Algarni and Nutter, 2015) and white-topping methods (Krispel et al., 2017). A combination of these measures is referred to hereinafter as the “White City”.

2.4.2. Green evaporating surfaces

Another set of climate adaptation measures is the enhancement of low (grass)/high (trees) vegetated areas or the addition of green roofs. In this case, the fractions of low vegetated areas and the number of trees, especially in public areas (LU classes 8 to 10 and 15 to 17 as given in Fig. 2), but also for (private) buildings around the city core (LU classes 3 to 5 and 7) were considered.

The first measure is the reduction of sealed areas f_p, which implies an increase in the fraction of low vegetated areas f_v and the remaining unvegetated, pervious areas. Therefore, the impervious areas were reduced by 30% of the given value and the compensatory f_v was increased at the same rate as f_p in LU classes 1 to 6 but not in LU class 7 (since industry and military units will not be able to implement these changes due to the need for impervious surfaces). The percentage of unvegetated, pervious areas remained unchanged.

The second and currently popular adaptation measure is the installation of green roofs (mostly on new buildings with flat roofs). Due to the tremendous costs of adding green roofs to older buildings (in our case LU classes 1 and 2), we considered only green roof additions to LU classes 3 to 5 and 7. The fraction of green roofs was set to 50% of the roof area with a semi-intensive soil depth of 25 cm.

The third measure considered an increase in the number of trees by 50% of the given value σ_t in the previously mentioned LU classes in public areas. The fourth measure included an increase in f_v. Hence, unvegetated, pervious areas disappear (e.g., grass instead of cobblestone) while sealed areas remain at the same value. The last green adaptation measure is based on afforestation in combination with the climatic influence of Lake Wörthersee (LU class 27 in Fig. 2a and b) and the prevailing onshore breeze from the lake towards the city during the daytime. Additional forest with an area of 1.4 km^2 in the southwestern part of the domain was added in the model, replacing areas currently under annual crops.

The combination of all green adaptation measures is referred to hereinafter as the “Green City”.

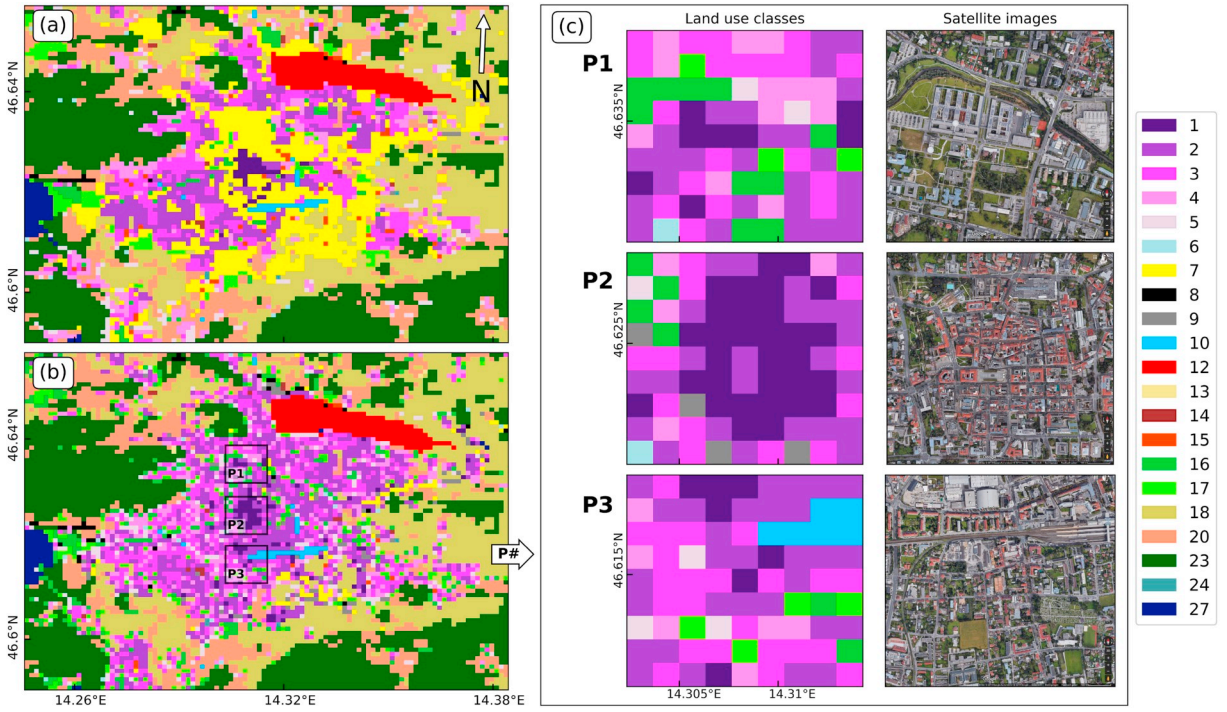

Fig. 2. Land use classification for the urban area of Klagenfurt (a) for the initial Urban Atlas map and (b) after the applied threshold method based on zonal statistics and land cover data from the Land Information System Austria (LISA) with a spatial resolution of 100 m. Panel (b) shows three small areas (P1, P2 and P3) enlarged in panel (c) with land use classes and satellite images (Source: Google, 2019). P1 to P3 are areas of interest regarding climate adaptation measures (evaluated in Section 3.4). Land use classification: 1 - Continuous urban fabric; 2 - Discontinuous dense urban fabric; 3 - Discont. medium density urban fabric; 4 - Discont. low density urban fabric; 5 - Discont. very low density urban fabric; 6 - Isolated structures; 7 - Industrial and military units; 8 - Transit roads and assoc. land; 9 - Other roads and assoc. land; 10 - Railways and assoc. land; 12 - Airport; 13 - Mineral extraction; 14 - Construction sites; 15 - Land without current use; 16 - Green urban areas; 17 - Sports and leisure facilities; 18 - Annual crops; 20 - Pastures; 23 - Forests; 24 - Moors; 27 - Water. (For interpretation of the references to colour in this figure legend, the reader is referred to the web version of this article.)

3. Results

3.1. Land cover improvements with TCM and the impact on climate model results

Based on the TMC introduced in Section 2.2.1, a new LU map was created for Klagenfurt and the surrounding districts (see Fig. 2b) and compared with the initial LU map of the UA (see Fig. 2a). The UA mapping and classification was checked and corrected, e.g., widespread industrial units (LU class 7) were substituted by common residential areas (according to IPAK). Additionally, the comparison revealed that several green urban areas were missing in the initial LU map. LU classes like railways (10), annual crops (18) or pastures (20), which are difficult to separate from other pervious areas, remained as given in the UA.

In addition, three areas of interest (P1, P2 and P3) were chosen as study anchor points to investigate their potential for decreasing the spatial averaged air temperature $\overline{T}_a$. These locations where chosen based on their importance for citizens (i.e., highly frequented places) and the relevance for (possible) heat stress situations (Fig. 2c). P1 represents the recently built hospital and the surrounding areas such as a green urban park and a small shopping center. The historic downtown, shown as P2, is the primary target for tourists in Klagenfurt. P3 marks the main train station (LU class 10) as well as the city hall (LU class 1 in the upper part of the section).

The spatial pattern and intensity of the urban heat load, and the climate indices, in particular, depend strongly on the LU distribution and the related properties of the LU classes in the urban climate simulations. The improvement in the detail of the LU map results in different distributions of the climate indices. Fig. 3a and b show, respectively, the comparison between the initial UA classification and the map after applying the TMC proposed here. While the UA-based model results show some areas (mainly in the outskirts) with almost the same values of heat load, the TMC-based results show strongly increased $\overline{HD}\ y^{-1}$ in the same parts (especially in the north and east part of the city center).

However, a closer comparison reveals structural differences across the whole domain of the city. Fig. 3c shows the difference in model results between the UA- and TMC-based LU classifications whereas areas exist that yield an increase of up to 7.4 $\overline{HD}\ y^{-1}$, which is about a 40% difference. These areas have a denser building structure in the TMC than the UA classification. Moreover, a few areas showed differences of opposite signs of up to − 6.5 $\overline{HD}\ y^{-1}$ (about a 36% difference), predominantly in the western part of Klagenfurt.

The same comparison but for $\overline{SD}\ y^{-1}$ is given in Fig. S4 in the Supplementary Material showing similar “cooling” and “heating” effects.

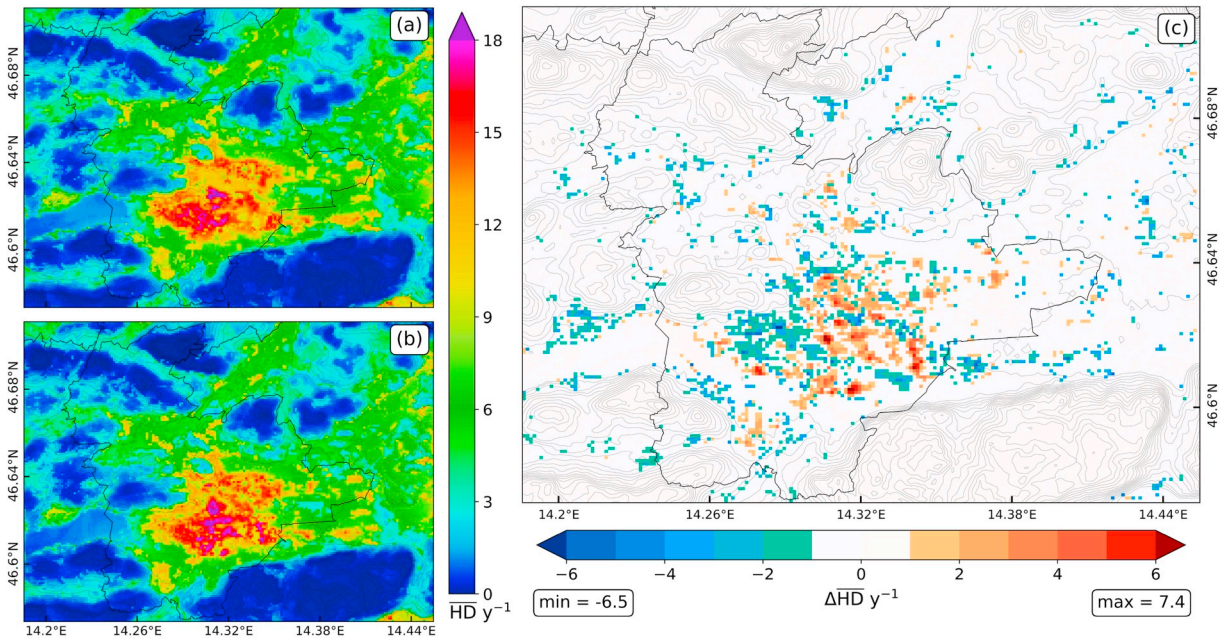

Fig. 3. Average number of hot days per year ($\overline{HD}$ y^{-1}) between 1981 and 2010 for simulations considering (a) the initial Urban Atlas map and (b) the proposed land use classification after the applied threshold method. Panel (c) provides the difference ($\Delta\overline{HD}$ y^{-1}) in the simulations in panels (a) and (b). For reference, the minimum and maximum values of $\Delta\overline{HD}$ y^{-1} are given beneath the colorbar in panel (c).

3.2. Reference simulations

To validate the model performance, we used the climate indices $\overline{SD}$ y^{-1} and $\overline{HD}$ y^{-1} calculated for the time periods 1971–2000 and 1981–2010 and compared them with the observed values at the weather station at Klagenfurt Airport. Due to the reliability of the measurements needed for the validation, only one long-term monitoring weather station was available in the study domain.

Table 3 shows the values obtained from the reference simulation (SIM) compared to the measurements (OBS) for $\overline{SD}$ y^{-1} and $\overline{HD}$ y^{-1}. For $\overline{SD}$ y^{-1} from 1971 to 2000, SIM shows a difference of −4% compared to OBS while the second time period provides the best result with −1%. Due to the lower absolute values of $\overline{HD}$ y^{-1}, the percentage deviation of −17% (1971–2000) and −13% (1981–2010) is much higher than the values of $\overline{SD}$ y^{-1} but the results are considered to have good accuracy when compared to Früh et al. (2011). We hypothesize that the increased difference between the two time periods stems from urban growth in the last decades. Unfortunately, the lack of historical land use and comparative meteorological data does not allow for a precise evaluation.

The reference climate indices were mapped in Fig. 4, which shows the spatial distribution of $\overline{SD}$ y^{-1} (panel (a)) and $\overline{HD}$ y^{-1} (panel (b)) for 1981–2010. On closer examination, Fig. 4b reveals two larger urban areas where $\overline{HD}$ y^{-1} is above 18. These areas represent mainly the historic downtown and the city hall (P2 and P3 enlarged in Fig. 2c).

3.3. Future climate scenarios

In order to analyze the interaction between regional climate change and the urban environment, we analyzed the climate change signal from the EURO-CORDEX model runs and climate indices based on urban climate model simulations.

In the case of regional climate signals, under RCP4.5, the average air temperature $\mu(T_a)$ increases by about 1.2 °C until the end of the 21th century compared to the reference time period 1981–2010 (Fig. 5a). Under RCP 8.5, the increase in $\mu(T_a)$ is more than double at 3.0 °C by 2100 compared to RCP4.5 (Fig. 5b). The red histogram in Fig. 5b also indicates that average daily air temperatures of 30

Table 3
Results of the reference simulations (SIM) compared to measurements from the weather station at Klagenfurt Airport (OBS) regarding the average number of summer ($\overline{SD}$) and hot days ($\overline{HD}$) per year for the time periods 1971–2000 and 1981–2010. The relative difference (Bias) for each time period and the modified index of agreement (d_1 defined by Willmott et al. (1985)) are given in the third and fourth column.

	1971–2000				1981–2010			
CI	OBS	SIM	Bias	d_1	OBS	SIM	Bias	d_1
$\overline{SD}$	54.6 ± 11.8	52.5 ± 14.0	−4%	0.75	62.8 ± 12.8	62.4 ± 14.2	−1%	0.77
$\overline{HD}$	8.8 ± 7.7	7.3 ± 7.5	−17%	0.86	14.0 ± 9.4	12.2 ± 9.0	−13%	0.86

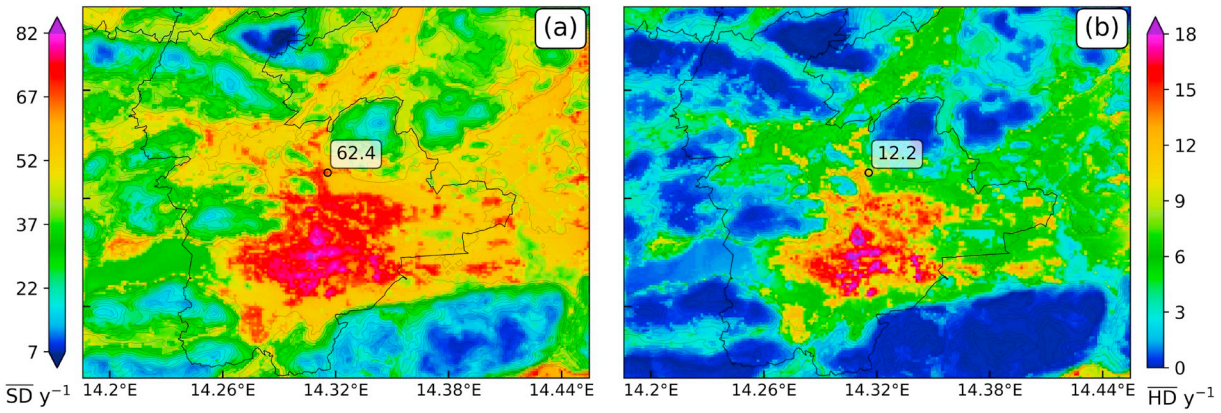

Fig. 4. Reference simulations of the average number of (a) summer and (b) hot days per year ($\overline{SD}$ y^{-1} and $\overline{HD}$ y^{-1}) for the time period 1981–2010 with modeled values indicated near the weather station at Klagenfurt Airport.

°C and greater will occur in case of RCP8.5 until 2100.

Further analysis of the spatial distribution in Klagenfurt based on urban climate model runs reveals more distinct impacts of climate change in terms of hot days. Fig. 5c to f provide the difference in $\overline{HD}$ y^{-1} for each RCP scenario and future time period compared to 1981–2010. While the increase in $\overline{HD}$ y^{-1} in urban areas (inner districts) is quite similar until the middle of the 21st century (panels (c) and (e)), the increase between 2071 and 2100 is extremely high, not only for urban environments, but also for suburban areas. Fig. 5d and f show that the number of hot days is larger inside (sub)urban areas than in rural areas. For example, in RCP4.5, there is a difference of approximately 8 $\overline{HD}$ y^{-1} between urban and rural environments, while in RCP8.5, this difference increases to around 12 hot days per year.

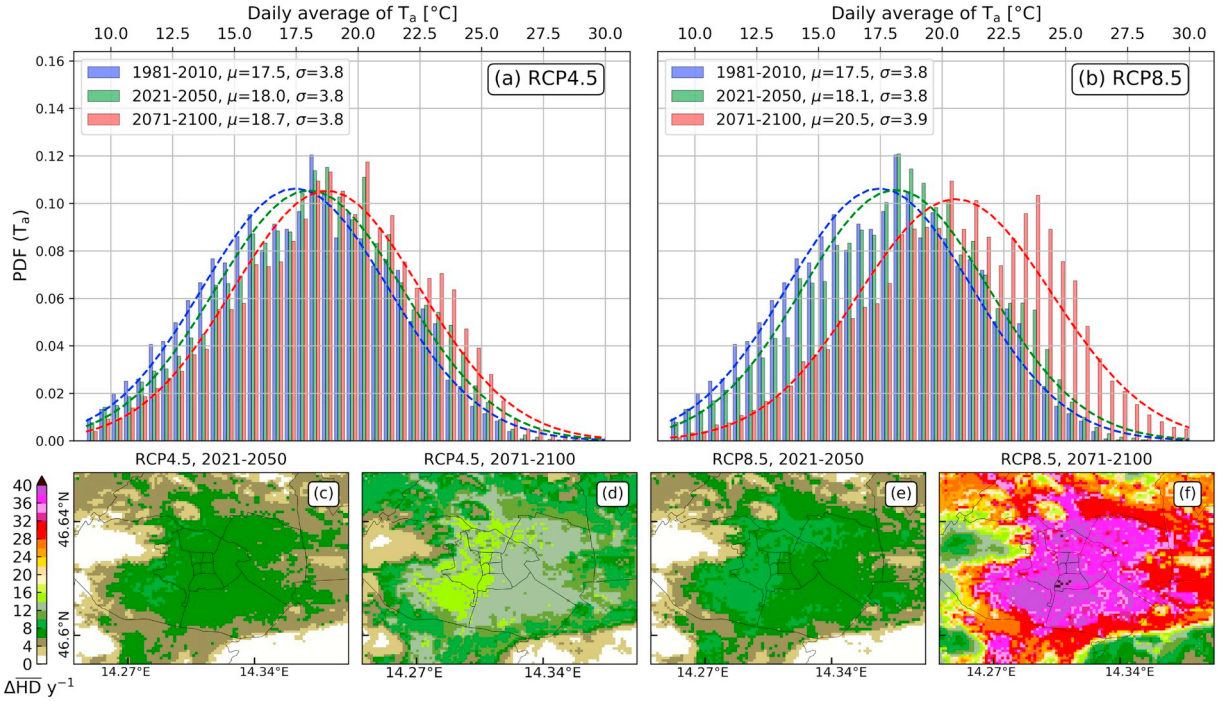

Fig. 5. Future climate projections shown as a probability density function (PDF) of the air temperature (T_a) taken from the bias-corrected EURO-CORDEX data set for Representative Concentration Pathways (RCP) of (a) RCP4.5 and (b) RCP8.5 for the extended summer season (MJJAS). Panels (a) and (b) provide histograms and a Gaussian normal distribution for the time periods 1981–2010 (blue), 2021–2050 (green) and 2071–2100 (red) with the average value (μ) and standard deviation (σ), respectively. The difference in the average number of hot days per year ($\Delta\overline{HD}$ y^{-1}) compared to 1981–2010 is shown for each time period for RCP4.5 in panels (c) and (d) and for RCP8.5 in panels (e) and (f). (For interpretation of the references to colour in this figure legend, the reader is referred to the web version of this article.)

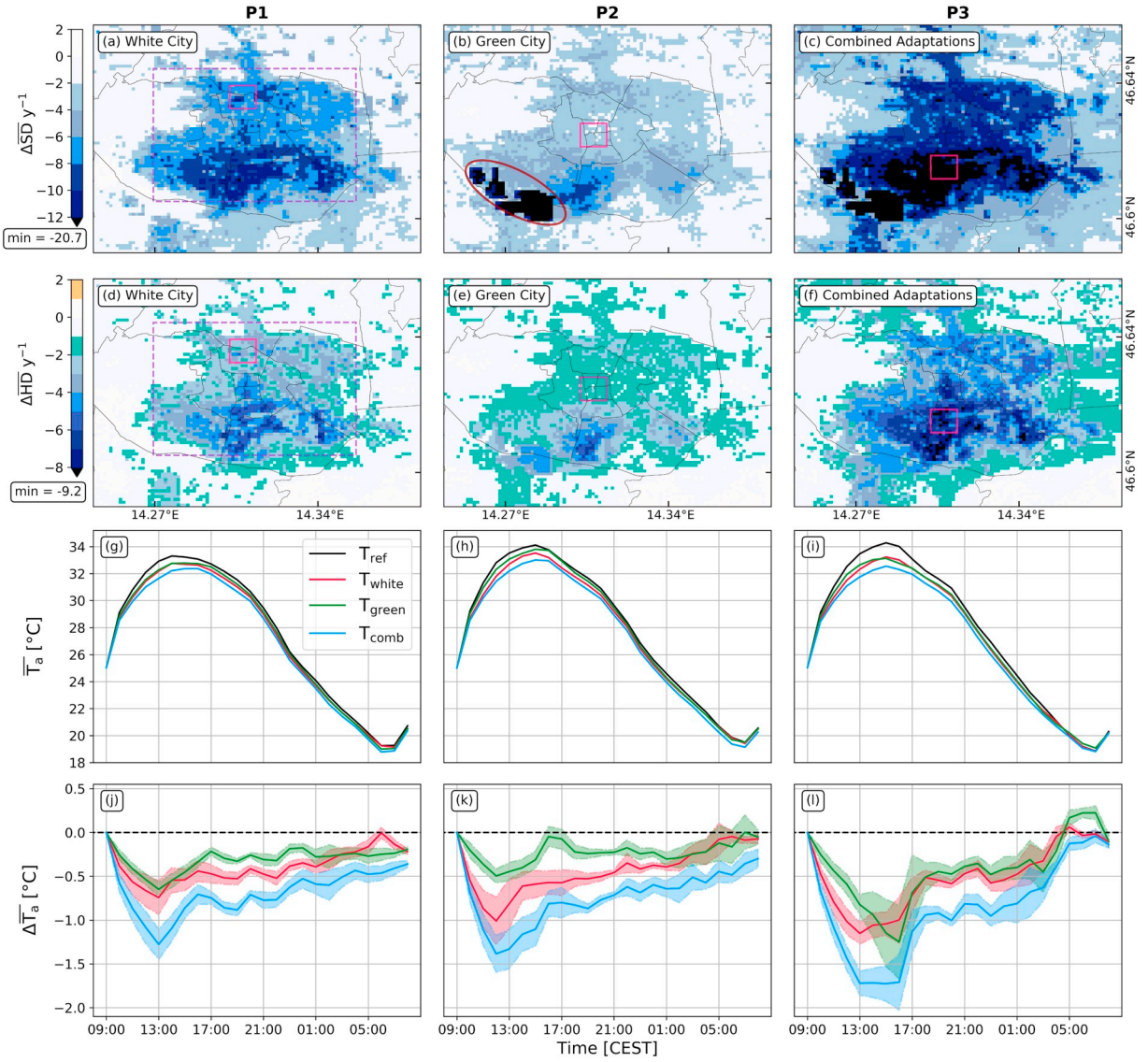

Fig. 6. Evaluation of the different climate adaptation measures for the urban area of Klagenfurt and three small areas (P1, P2 and P3) as shown in Fig. 2c. Panels (a)-(c) show three combined adaptation measures corresponding to the "White City", the "Green City" (see Section 2.4) and an overall "Combined Adaptation" ("White City" and "Green City" together) regarding the difference in the average number of summer days per year ($\Delta\overline{SD}$ y^{-1}) compared to the reference simulation for the time period 1981–2010. Panels (d)-(f) are the same as (a)-(c) but show the number of hot days per year ($\Delta\overline{HD}$ y^{-1}). The minimum values of $\Delta\overline{SD}$ y^{-1} and $\Delta\overline{HD}$ y^{-1} are shown beneath the colorbar, respectively. The purple dashed square in panel (a) and (d) marks the area of averaged values in Table 4. The dark red ellipse in panel (b) marks the afforestation as one of the adaptation measures. Panels (g)-(i) show the average air temperature ($\overline{T_a}$) of the reference simulation (T_{ref}), "White City" (T_{white}), "Green City" (T_{green}) and "Combined Adaptation" (T_{comb}) within the areas of interest (P# marked as magenta solid squares in panels (a)-(f)). Panels (j)-(l) show the difference in air temperatures ($\Delta\overline{T_a}$) and the corresponding standard deviation (marked as shaded region) between the individual adaptation measures and the reference simulation, respectively. (For interpretation of the references to colour in this figure legend, the reader is referred to the web version of this article.)

3.4. Climate adaptation measures for current climate conditions

Historical trend analysis and future climate projections have shown that adaptation measures are necessary regardless of which RCP scenario will be realized over this century. The simulation of the climate for 1981–2010 is considered as a reference case (see Fig. 4), and all simulations with their individual/combined adaptation measures are compared against this reference case. In addition to the climate indices, we analyzed $\overline{T_a}$ in the areas of interest. For this purpose, we selected the idealized daily simulation from MUKLIMO_3 where the heat load was the strongest such as on a clear-sky day with low humidity and low wind speed conditions (i.e., C_{100} (T_{cmax}, rh_{cmin}, v_{cmin}) as given in Fig. S2 in the Supplementary Material).

Table 4
Absolute (average (Avg.) values inside the orchid dashed square in Fig. 6a and minimum (Min.) values in the study domain) and relative (%) differences in the number of summer days ($\Delta\overline{SD}$ y^{-1}) and hot days ($\Delta\overline{HD}$ y^{-1}) per year for the simulation of the climate adaptation measures (change in roof albedo α_r, wall albedo α_w, street albedo α_{st}, fraction of impervious areas f_p, number of trees σ_t, fraction of low vegetated areas f_v; a combination of lines 1 to 3 as the so-called " White City", a combination of lines 4 to 8 as the so-called "Green City", and an overall combined simulation) compared to the reference simulation from 1981 to 2010, respectively. Values marked in light green indicate statistically significant differences (Mann-Whitney *U* Test with 99% confidence interval, N = 2835) compared to the reference simulation. Note that the percentage decrease or increase in f_p and σ_t indicates a relative change for the given land use class.

	$\Delta\overline{SD}$ y^{-1}				$\Delta\overline{HD}$ y^{-1}			
Adaptation measures	Avg.	%	Min.	%	Avg.	%	Min.	%
Increase α_r $(0.2 \rightarrow 0.5)$	-2.7 ± 1.1	-4.1	-6.4	-8.4	-1.4 ± 0.7	-11.0	-4.0	-20.7
Increase α_w $(0.3 \rightarrow 0.5)$	-0.9 ± 0.7	-1.4	-3.3	-4.3	-0.5 ± 0.3	-4.1	-2.0	-10.1
Increase α_{st} $(0.2 \rightarrow 0.4)$	-2.1 ± 1.0	-3.2	-5.6	-7.3	-1.1 ± 0.6	-8.9	-3.3	-17.1
Decrease f_p (-30%)[1]	-1.2 ± 0.6	-1.7	-3.0	-4.2	-0.8 ± 0.4	-5.8	-2.3	-12.8
Add green roofs (0.50)	-1.3 ± 0.8	-1.9	-4.7	-6.5	-0.6 ± 0.4	-5.2	-2.5	-17.1
Increase σ_t $(+50\%)$[1]	-0.5 ± 0.6	-0.7	-3.5	-8.2	-0.3 ± 0.3	-2.3	-1.7	-20.2
Remove unvegetated, pervious area[2]	-0.7 ± 0.5	-1.0	-2.7	-4.9	-0.5 ± 0.4	-4.1	-2.2	-12.2
Afforestation in the southwest	-0.4 ± 2.4	-0.6	-7.6^*	-10.0^*	-0.2 ± 1.0	-1.7	-4.9^*	-27.1^*
'White City'	-6.5 ± 2.6	-9.8	-12.3	-15.3	-2.9 ± 1.5	-24.8	-7.3	-37.8
'Green City'	-4.1 ± 2.3	-5.9	-9.7^*	-14.3^*	-2.0 ± 1.1	-17.3	-6.7^*	-35.8^*
Combination	-9.3 ± 3.4	-14.6	-16.2^*	-20.8^*	-4.2 ± 1.8	-35.7	-9.2^*	-44.0^*

[a] Values refer to the land use classes given in Tables 1 and 2.
[b] Use as f_v instead.
* Minimum values are given within urban environments while the overall minimum values are located partially in the forest (see Fig. 6 and Fig. S13a in the Supplementary Material).

All the results that were evaluated over a specific area (i.e., the whole city marked as purple dashed square in Fig. 6a and d (N = 2835) or areas of interest (N = 81)) have been checked for statistical significance (see Tables 4 and 5 for further information).

3.4.1. "White City"

Table 4 shows the results for different climate adaptation measures expressed as the change in the climate indices. A clear decrease in the urban heat load is shown, particularly in the case where α_r yielded the lowest values (i.e., the highest potential) on average as well as for the maximum reduction (line 1 in Table 4). The second largest decrease is shown in the case of increasing α_{st} (line 3 in Table 4), where values for $\Delta\overline{SD}$ y^{-1} vary around an average of -2.1 and for $\Delta\overline{HD}$ y^{-1}, around an average of -1.1. The weakest effect from the albedo adaptation measures showed an increase in the value of α_w, which was around half of α_r and α_{st} (line 2 in Table 4). Nevertheless, each measure produces a difference that is statistically significant (marked in light green in Table 4) compared to the reference case.

The combination of α_r, α_w and α_{st} ("White City") has more than just a cumulative impact on the UHI effects. The average and minimum values show a strong decrease across the climate indices (up to 37.8%), which are comparatively larger than a single, highly reflective adaptation measure. If we consider the average values of each "White City" adaptation, the effect of the combination is larger than the sum of the individual components (see Table 4 for $\Delta\overline{SD}$ y^{-1}). The reason could be the connection between each sealed surface and the resulting reduced heat transfer between them. Hence, the mitigation of heat loads is enhanced.

Fig. 6a and d provide the spatial distribution of these combined "White City" adaptation measures. The heat load is reduced under this assumptions by up to 12.3 $\overline{SD}$ y^{-1} and by up to 7.3 $\overline{HD}$ y^{-1} across the whole city. The "cooling" effect increases with a higher

Table 5
Difference in the average air temperature of the daily maximum (15:00–16:00 CEST) and minimum (06:00–07:00 CEST) values compared to the reference simulation from 1981 to 2010 (see Fig. 6j-l). Each combination of adaptation measures ("White City", "Green City", and an overall combination) is given within the areas of interest (P#). Values marked in light green indicate statistically significant differences (Mann-Whitney *U* Test with 99% confidence interval, N = 162) compared to the reference simulation.

	$\Delta\overline{T}_a$ $15-16^{00}$ CEST			$\Delta\overline{T}_a$ $06-07^{00}$ CEST		
Adaptation	**P1**	**P2**	**P3**	**P1**	**P2**	**P3**
'White City'	-0.5 ± 0.1	-0.6 ± 0.1	-1.0 ± 0.2	-0.1 ± 0.1	-0.1 ± 0.0	0.0 ± 0.0
'Green City'	-0.4 ± 0.1	-0.2 ± 0.2	-1.1 ± 0.4	-0.2 ± 0.1	-0.1 ± 0.2	$+0.2 \pm 0.1$
Combination	-0.8 ± 0.1	-1.0 ± 0.2	-1.7 ± 0.3	-0.4 ± 0.1	-0.4 ± 0.1	-0.1 ± 0.1

density of urban fabric (e.g., in the southern part of the city center).

Considering the areas of interest (P1, P2 and P3) and their potential to reduce the urban heat loads on local scale with this combined adaptation measure, the averaged ambient air temperature with increased reflectivity T_{white} (see Fig. 6g-i) decreases locally by up to 0.7 ˚C for P1, up to 1.0 ˚C for P2 and up to 1.2 ˚C for P3 at around 13:00 CEST (maximum solar incidence) as shown in Fig. 6j-l. The same procedure that was used to determine statistical significance for the climate indices was applied to the air temperature within those areas. Therefore, we use the time period of the daily maximum and minimum values of the $\overline{T_a}$ (see Table 5). In the case of the "White City", $\Delta\overline{T_a}$ varies between −0.4 and −1.2 ˚C for the highest daily temperatures (which are significantly different to the reference), but reach almost no "cooling" effect in the morning. We see that highly reflective surfaces inside urban environments are beneficial only during the daytime. A further evaluation of each "White City" adaptation measure with respect to $\overline{T_a}$ is provided in the Supplementary Material (see Fig. S5-S7).

3.4.2. "Green City"

As outlined in Section 2.4.2, certain green surfaces were implemented in MUKLIMO_3 to evaluate their potential to mitigate urban heat loads. Table 4 indicates that the effect of such measures varies between a slight decrease in the climate indices (maximum reductions of up to 1.9% for $\Delta\overline{SD}$ y^{-1} and up to 5.8% for $\Delta\overline{HD}$ y^{-1}) in the average and a locally strong "cooling" effect with maximum reductions up to 10.0% for $\Delta\overline{SD}$ y^{-1} and 27.1% for $\Delta\overline{HD}$ y^{-1}, respectively. The evaluation of the statistics for the average values results in the fact that the afforestation (marked as a dark red dashed ellipse in Fig. 6b) in the southwestern part of the domain has no significant effect on the whole city although the highest local "cooling" values come from this measure. The reason for this positive microclimatic effect is the prevailing wind direction (WSW) in that area, leading to the advection of "cooler" air masses from the afforestation towards the city (see Fig. S13c in the Supplementary Material where the air temperature decreases rapidly by more than 1.0 ˚C). A similar result can be observed when increasing the number of trees by 50% within (sub)urban environments. While the decrease in the climate indices is, on average, only for $\Delta\overline{HD}$ y^{-1} statistically significant (-0.3 ± 0.3), the maximum reduction reaches 20.2%. This effect of averaging over a larger region is also shown in the areas of interest. Whereas $\Delta\overline{T_a}$ varies around 0.0 ˚C on average inside P1, P2 and P3 (see Fig. 10c in the Supplementary Material), the "cooling" effect, which occurs only in LU classes 16 and 17 (i.e., spaces where $\sigma_t \geq 50\%$), results in reductions of up to 0.3 ˚C (see Fig. S11c in the Supplementary Material). In conclusion, trees have a strong impact at the local scale, whereas low vegetated areas (on the ground and/or at roof level) have more spatial potential to reduce the effect of the UHI (i.e. stronger reduction in the average values).

Finally, we simulated a combination of the "Green City" adaptation measures, which is shown in Fig. 6b and e. Here, a cumulative reduction in heat loads over the whole city emerges, but the effectiveness of these measures does not appear to be as pronounced as those from the "White City" (except for the southern part of the domain, which is mainly due to the aforementioned afforestation area). However, the average and maximum reductions show a clear (and significant) decrease in the magnitude of the climate indices with −5.9% and −14.3% for $\Delta\overline{SD}$ y^{-1} and −17.3% and −35.8% for $\Delta\overline{HD}$ y^{-1}, whereas the maximum reductions are close to those from the "White City" (e.g., compare lines 9 and 10 in Table 4). If we focus on the areas of interest and their air temperatures T_{green} (see Fig. 6g-i), we further note in Fig. 6j-l that the outputs are always higher than those from T_{white} (except in the afternoon in P3 where $\Delta\overline{T_a}$ yields a maximum reduction of up to 1.3 ˚C at 16:00 CEST). The statistical analysis reveals an ambivalent result. While the air temperature decreases significantly in all areas of interest during the daytime (partially lower than the "White City"), $\Delta\overline{T_a}$ increases significantly up to 0.2 ˚C in P3 until the morning (around 06:00 CEST). This increase results from the afforestation (explained by the reduced wind speeds from the city towards Lake Wörthersee, i.e., reversed onshore breezes during the nighttime) and the fact that green roofs have better insulation on a clear night with enhanced upward longwave radiation (see Fig. S9 and S13 in the Supplementary Material).

3.4.3. Combination of all climate adaptation measures

As a last scenario, we considered the pooling together of individual climate adaptation measures, as we were interested in quantifying the overall mitigating potential on UHI effects. This scenario combines all previous adaptation steps. We note that the combination of white and green roofs means that half the roof area has an albedo value of 0.5 while the other half implies a green roof as described in Section 2.4.2. Fig. 6c and f show the strongest decrease in $\Delta\overline{SD}$ y^{-1} and $\Delta\overline{HD}$ y^{-1} with a maximum reduction of 16.2 and 9.2, respectively. Hence, $\overline{SD}$ and $\overline{HD}$ could be reduced under such a scenario by up to 20.8% and 44.0%, respectively, in the southern part of Klagenfurt (see Table 4 for further information). The average ambient air temperature T_{comb} for our areas of interest P1, P2 and P3 show a pronounced decrease over the full 24 h daily cycle, reaching up to −1.3 ˚C (Fig. 6j), up to −1.4 ˚C (Fig. 6k) and up to −1.7 ˚C (Fig. 6l), respectively. A closer look at $\overline{T_a}$ reveals that the overall combination approximately reaches the sum of the "White City" and "Green City" during the daytime and is the only option that reduces the ambient air temperature (by up to −0.4 ˚C) in every area of interest (with statistically significant differences) during the nighttime (see Table 5).

These results indicate that some climate adaptation measures show higher potential in mitigating the effects of the UHI than others. The potential of each adaptation measure to reduce the urban heat load in Klagenfurt during the daytime (with statistical significance) varies between 2.3% and 11.0%, but a combination of several measures can yield a cumulative reduction varying from 17.3% (green adaptations) through to 24.8% (white adaptations) and up to 35.7% (overall combined adaptations) for $\Delta\overline{HD}$ y^{-1} as an average over the whole city.

3.5. Climate adaptation measures for future climate conditions

In these examples, the proposed adaptation measures are shown in combination with possible future climate change scenarios

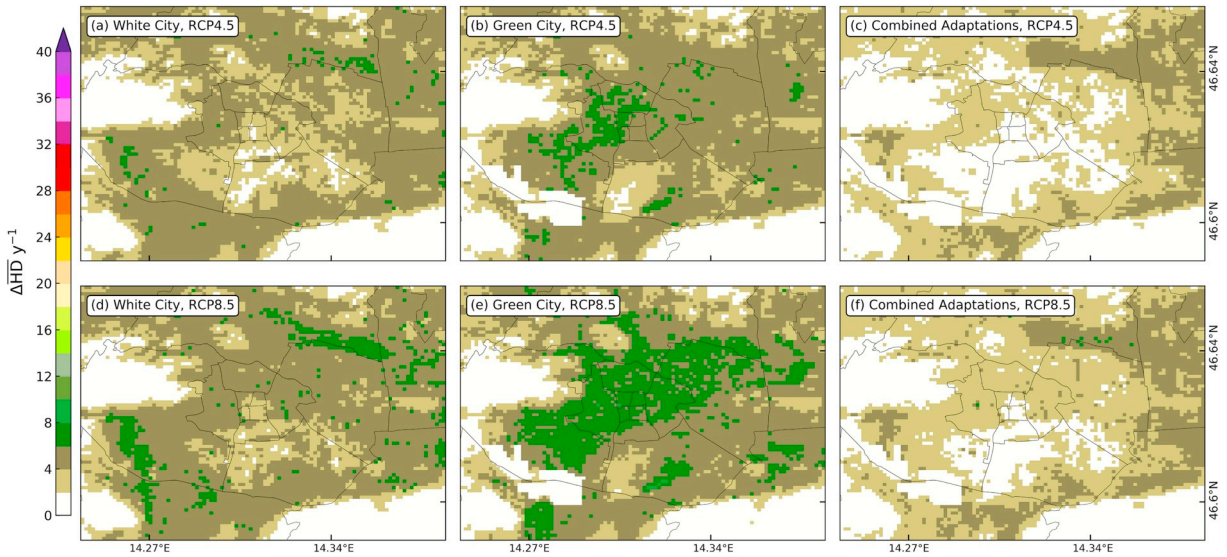

Fig. 7. Same as Fig. 6d-f but this shows the future climate projections for Representative Concentration Pathways (RCP) of (a)-(c) RCP4.5 and (d)-(f) RCP8.5 for the time period 2021–2050.

(RCP4.5 and RCP8.5). As future land cover and LU changes are not known, the scenarios are evaluated based on the current urban structure in Klagenfurt.

3.5.1. Time period 2021–2050

The results for both RCPs regarding $\overline{HD}\ y^{-1}$ for the time period between 2021 and 2050 (see Fig. 7) show general increases compared to the reference case 1981–2010. In contrast to Fig. 5c and e where an increase of $\geq 8\ \Delta\overline{HD}\ y^{-1}$ occurs, the "White" and "Green City" scenarios can lead to a reduction in urban heat loads varying between 0 and 7.9 $\Delta\overline{HD}\ y^{-1}$. However, the strongest "cooling" effect is achieved with a combination of white and green adaptation measures. Furthermore, the whole city has lower values in $\overline{HD}\ y^{-1}$ than the area around the airport (see Fig. 2 with LU class 12) and parts in the south and east of the city, i.e., urban heat loads during the daytime could be reduced or even disappear (compare with Fig. 4b). This result shows that the heat load during the daytime remains at approximately the same level as the current climate situation if one considers RCP4.5 until the middle of the 21st century.

The same analysis was also undertaken for the average number of summer days (see Fig. S14 in the Supplementary Material). Panels (c) and (f) show a similar effect as before, where parts of the city remain at the level of current climate conditions.

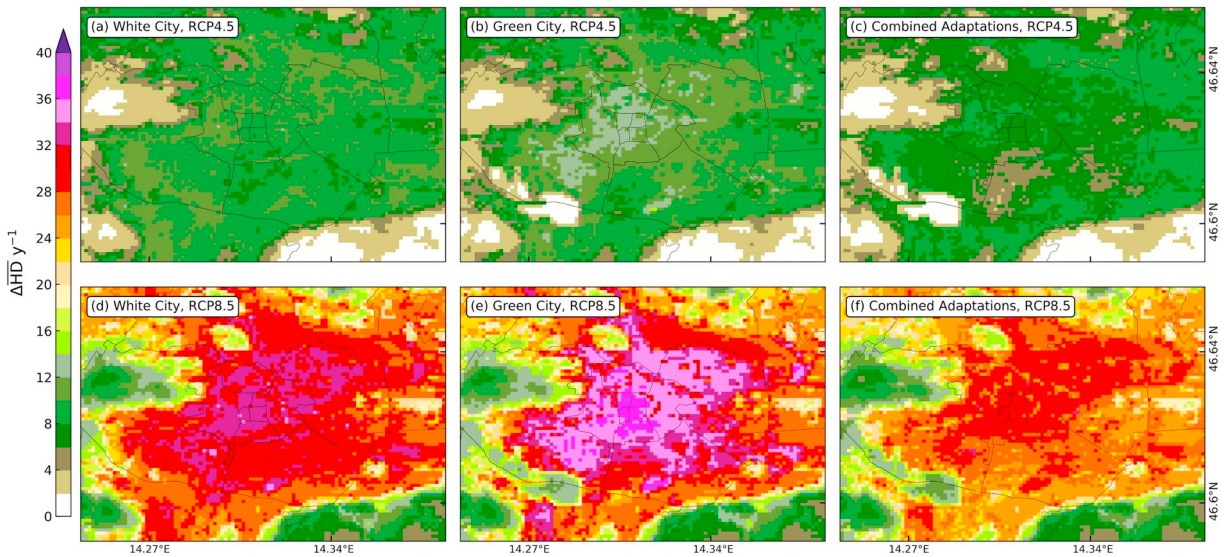

Fig. 8. Same as Fig. 7 but for the time period 2071–2100.

3.5.2. Time period 2071–2100

By the end of the 21st century for the worst case scenario (RCP8.5), the number of $\overline{HD}$ y^{-1} would yield values around 60 in the city core (see Fig. 5f). In Fig. 8, a similar "cooling" effect as for 2021–2050 (Fig. 7) is visible by comparing the results without and with several adaptation measures. Regarding RCP8.5, the "White City" and the "Green City" have only minor mitigation potential for reducing the heat load to present day levels (i.e. varying between 30 and 38 for $\Delta\overline{HD}$ y^{-1}). The overall combination of adaptation measures can reduce the increase in $\overline{HD}$ y^{-1} to a value of ≤ 30 (see Fig. S15 for similar results but for $\overline{SD}$ y^{-1}), which is still very high compared to the reference period.

These additional results for future scenarios indicate that in case of RCP8.5, any combination of adaptation measures will not reduce UHI effects enough by 2100. However, if CO_2 emissions are reduced sufficiently (i.e. in case of RCP4.5), an increase in climate indices will be mitigated to lower levels as for rural areas with a combined implementation of all the adaptation measures.

4. Discussion and conclusions

This study investigated the potential of climate adaptation measures to mitigate UHI effects for the city of Klagenfurt, Austria. For this purpose, we used a set of targeted scenario simulations performed with the microscale urban climate model MUKLIMO_3, in conjunction with the cuboid method, to derive information on long-term changes of climatological indices relevant to heat exposure during the daytime such as $\overline{SD}$ y^{-1} and $\overline{HD}$ y^{-1}.

The LU information required by the urban climate model was initially built from data in the UA. Information from LISA was used to evaluate the urban and rural classification properties and to reclassify the LU types of the UA data set. For this reclassification, we demonstrated a novel procedure, referred to as TMC. Based on the available data from LISA and precise local information on building heights, the TMC allowed a more accurate LU map of the study domain to be derived. Climate indices derived from a set of urban microclimate model runs using the TMC LU information served as a baseline simulation (1981–2010). This simulation was used as a reference for the analysis of future climate scenarios until 2100 and to investigate the effectiveness of individual, multiple and overall combined adaptation measures.

We evaluated the effectiveness of different climate adaptation measures by comparing the heat load changes with the reference simulation. These adaptation measures contained two types of adaptation strategies: (i) enhanced albedo values of sealed areas (roof albedo increased from 0.2 to 0.5, wall albedo increased from 0.3 to 0.5 and street/sidewalks albedo increased from 0.2 to 0.4) and (ii) highly evaporating green surfaces/areas (decrease in sealed areas by 30%, green roofs implemented for 50% of the roofs, number of trees increased by 50%, low vegetated areas increased, and afforestation with an area of 1.4 km^2 near the city).

While different climate adaptation measures are known to reduce the heat load in urban environments, there are also some challenges associated with increasing the overall thermal comfort through such adaptation measures. Some studies document that enhanced albedo values of sealed areas can lower the ambient air temperature T_a (e.g., Synnefa et al. (2008)). Cool roofs have been shown in Santamouris (2014) and Straka and Sodoudi (2019) to reduce T_a in an urban canyon on average by 0.2 °C per 0.1 increase in the albedo value. Our results generally corroborate the findings of these studies, yielding a reduction of up to 0.65 °C with an increase of 0.3 in the albedo of roofs. Furthermore, the study of Jandaghian and Akbari (2018) showed that increased albedo values of all sealed areas (from 0.2 to 0.65, 0.6 and 0.45 for roof, wall and street, respectively) decrease not only T_a by up to 2.3 °C in urban environments, but also improve air quality in terms of ozone, nitrogen dioxide and fine particulate matter. These findings compare well with the results for T_a reduction in this study, showing that with the increase of reflectivity, the urban heat load decreases. On the contrary, several studies report on thermal discomfort (e.g., Taleghani (2018)) due to highly reflective surfaces (depending on position and orientation) and hence, an increased mean radiant temperature. Such thermal comfort indices and their strong spatial variations (i.e., at 1 m resolution), especially within complex urban environments as described in Lindberg et al. (2013), would create too much uncertainty considering the comparatively coarse resolution of the MUKLIMO_3 model (i.e., with spatial resolutions of 20 to 100 m in this study) and hence are not discussed in the paper. However, local governments and urban planners should find a good compromise between highly reflective surfaces to decrease T_a and the overall thermal comfort.

Even though green roofs are considered to have a positive effect in reducing the urban heat load, the effectiveness of green roofs located on high buildings in reducing T_a at the pedestrian level is under question. Zhang et al. (2019) showed recently that green roofs covering 25% or more of the roof with a building height lower than 60 m have an influence on T_a in an urban canyon (at a 1.4 m height above ground level). Specifically, at a 50% coverage and a building height of 10 m, the decrease in T_a was up to 0.44 °C which is similar to our results in P3 where the building height varies between 8 and 9 m.

Recently, Lindberg et al. (2016) and Ali and Patnaik (2019) showed that T_a, mean radiant temperature and heat stress can be reduced effectively at the local scale through increased tree coverage. On the other hand, Monteiro et al. (2016) showed that very small green spaces (areas less than 0.5 ha, which is the case in our study except for LU classes 16 and 17) did not bring substantial reductions in T_a. Our results show that an increase in the city wide number of trees yields an averaged difference in ΔT_a varying between ± 0.10 °C in all three areas of interest over the full 24 h daily cycle compared to the reference simulation. In contrast, the difference relative to the reference simulation shows a decrease by up to 0.31 °C on average within LU classes 16 and 17 (i.e. green urban areas). Hence, the increased number of trees, approximately 12.5% in LU classes 16 and 17, shows a similar value to that in Ali and Patnaik (2019) (0.03 °C decrease in the apparent temperature through an increase of tree density by 1%).

Although green adaptation measures can provide positive effects for the local climate, possible negative effects from the implementation of these measures should also be considered. It was shown that green adaptation measures (e.g., the installation of ornamental lawns) can yield an increase in greenhouse gas emissions between −108 and +285 g CO_2 m^{-2} y^{-1} associated with turfgrass maintenance (Townsend-Small and Czimczik, 2010). Another aspect that needs consideration in "city greening" is the

mortality of specific tree species. For Europe, it has been reported that during the last 35 years, the canopy mortality increased by 2.40% y^{-1} due to extreme climatic conditions such as droughts and/or bark beetle infestations (Senf et al., 2018). Such aspects must be considered (i.e. in a climate sustainable way) if there are plans to extend vegetated areas.

However, the strongest decrease in climate indices for the time period 1981–2010 was found for the adaptation measure with bright, reflective roofs, resulting in reductions of up to 8.4% for $\overline{SD}$ y^{-1} and 20.7% for $\overline{HD}$ y^{-1}. The largest difference for adaptation measures comprising vegetation was found through afforestation in the direct vicinity of the city of Klagenfurt, with reductions of 10.0% and 27.1% for $\overline{SD}$ y^{-1} and $\overline{HD}$ y^{-1}, respectively. As a combined measure scenario, we pooled all eight climate adaptation measures together. Such a scenario resulted in a pronounced decrease in both of the climate indices, i.e., maximum reductions of up to 20.8% for $\overline{SD}$ y^{-1} and 44.0% for $\overline{HD}$ y^{-1}.

Considering future climate projections, a tremendous increase in SD and HD will occur for both RCPs until the end of the 21st century. A reduced increase in these climate indices could be achieved over the next three decades (locally up to the current level) if highly reflective sealed surfaces are implemented. To remain at the current climate conditions for the whole city, a combined implementation of all the adaptation measures proposed here is necessary. Finally, the enhanced UHI effect until 2100 could be mitigated to lower levels (i.e., an increase of approximately 30 $\overline{HD}$ y^{-1} instead of 40 and greater) only with an overall combination of adaptation measures.

Our results show that a suite of climate adaptation measures can positively influence the thermal comfort in urban environments by reducing the heat load, and thus, the ambient air temperature. We see that a combination of adaptation strategies is the most effective in reducing the urban heat burden, and thus, it represents the most successful strategy for mitigating the effects of the UHI. However, we note in closing that any combination of adaptation measures will not reduce UHI effects enough by 2100 if CO_2 emissions are not reduced sufficiently.

Acknowledgement

The first author named is lead and corresponding author. All authors are part of the ADAPT-UHI project (KR17AC0K13693) team. This study was funded by the Austrian Climate Research Program (ACRP) as part of the ADAPT-UHI project (KR17AC0K13693). The authors thank the German Meteorological Service (DWD) for providing the MUKLIMO_3 model and for their continuous support. The authors are grateful to Harald Rieder and Philipp Weihs (University of Natural Resources and Life Sciences (BOKU), Vienna) for useful discussions.

Appendix A. Supplementary data

Supplementary data to this article can be found online at https://doi.org/10.1016/j.uclim.2020.100582.

References

Alexandri, E., Jones, P., 2008. Temperature decreases in an urban canyon due to green walls and green roofs in diverse climates. Build. Environ. 43 (4), 480–493. https://doi.org/10.1016/j.buildenv.2006.10.055. (Apr.).

Algarni, S., Nutter, D., 2015. Influence of dust accumulation on building roof thermal performance and radiant heat gain in hot-dry climates. Energy Build. 104, 181–190. https://doi.org/10.1016/j.enbuild.2015.07.018. (Apr.).

Ali, S.B., Patnaik, S., 2019. Assessment of the impact of urban tree canopy on microclimate in Bhopal: a devised low-cost traverse methodology. Urban Clim. 27, 430–445. https://doi.org/10.1016/j.uclim.2019.01.004. (Apr.).

Arnfield, A.J., 2003. Two decades of urban climate research: a review of turbulence, exchanges of energy and water, and the urban heat island. Int. J. Climatol. 23 (1), 1–26. https://doi.org/10.1002/joc.859. (Jan.).

Boé, J., Terray, L., Habets, F., Martin, E., 2007. Statistical and dynamical downscaling of the seine basin climate for hydro-meteorological studies. Int. J. Climatol. 27 (12), 1643–1655. https://doi.org/10.1002/joc.1602.

Bretz, S., Akbari, H., Rosenfeld, A., 1998. Practical issues for using solar-reflective materials to mitigate urban heat islands. Atmos. Environ. 32 (1), 95–101. https://doi.org/10.1016/s1352-2310(97)00182-9. (Jan.).

Chrysanthou, A., van der Schrier, G., van den Besselaar, E.J.M., Tank, A.M.G.K., Brandsma, T., 2014. The effects of urbanization on the rise of the european temperature since 1960. Geophys. Res. Lett. 41 (21), 7716–7722. https://doi.org/10.1002/2014gl061154. (Nov.).

Dessai, S., 2003. Heat stress and mortality in Lisbon part II. An assessment of the potential impacts of climate change. Int. J. Biometeorol. 48 (1), 37–44. https://doi.org/10.1007/s00484-003-0180-4. (Sep.).

D'Ippoliti, D., Michelozzi, P., Marino, C., de'Donato, F., Menne, B., Katsouyanni, K., Kirchmayer, U., Analitis, A., Medina-Ramón, M., Paldy, A., Atkinson, R., Kovats, S., Bisanti, L., Schneider, A., Lefranc, A., Iñiguez, C., Perucci, C.A., 2010. The impact of heat waves on mortality in 9 european cities: results from the EuroHEAT project. Environ. Health 9https://doi.org/10.1186/1476-069x-9-37. (Jul.).

European Union, 2018. Copernicus land monitoring service. In: European Environment Agency (EEA).

Früh, B., Becker, P., Deutschländer, T., Hessel, J.-D., Kossmann, M., Mieskes, I., Namyslo, J., Roos, M., Sievers, U., Steigerwald, T., Turau, H., Wienert, U., 2011. Estimation of climate-change impacts on the urban heat load using an urban climate model and regional climate projections. J. Appl. Meteorol. Climatol. 50 (1), 167–184. https://doi.org/10.1175/2010jamc2377.1. (Jan.).

Geletic, J., Lehnert, M., Dobrovolny, P., Žuvela-Aloise, M., 2019. Spatial modelling of summer climate indices based on local climate zones: expected changes in the future climate of Brno, Czech Republic. Clim. Chang. 1–16. https://doi.org/10.1007/s10584-018-2353-5.

Gidhagen, L., Olsson, J., Amorim, J.H., Asker, C., Belusic, D., Carvalho, A.C., Engardt, M., Hundecha, Y., Körnich, H., Lind, P., Lindstedt, D., Olsson, E., Rosberg, J., Segersson, D., Strömbäck, L., 2020. Towards climate services for european cities: lessons learnt from the copernicus project urban SIS. Urban Clim. 31, 100549. https://doi.org/10.1016/j.uclim.2019.100549. (Mar.).

Gill, S., Handley, J., Ennos, A., Pauleit, S., 2007. Adapting cities for climate change: the role of the green infrastructure. Built Environ. 33 (1), 115–133. https://doi.org/10.2148/benv.33.1.115. (Mar.).

Giorgi, F., Jones, C., Asrar, G.R., 2006. Addressing climate information needs at the regional lelvel: the cordex framework. In: Bulletin World Meteoroligal Organisation. 58.

GeoVille GmbH, 2016. Land Information System Austria (Lisa). Available from. https://www.landinformationsystem.at/#/lisa/overview (Accessed 18 September 2018).
Google Maps from the city of Klagenfurt, Accessed date: 18 September 2019.
Gross, G., 1989. Numerical simulation of the nocturnal flow systems in the freiburg area for different topographies. Beitr. Phys. Atmosph. 57–72 H 62.
Gross, G., 2012. Numerical simulation of greening effects for idealised roofs with regional climate forcing. Meteorol. Z. 21 (2), 173–181. https://doi.org/10.1127/0941-2948/2012/0291. (Apr.).
Gudmundsson, L., 2016. qmap: statistical transformations for post-processing climate model outputR package version 1.0–4.
Gudmundsson, L., Bremnes, J.B., Haugen, J.E., Engen-Skaugen, T., 2012. Technical note: downscaling RCM precipitation to the station scale using statistical transformations – a comparison of methods. Hydrol. Earth Syst. Sci. 16 (9), 3383–3390. https://doi.org/10.5194/hess-16-3383-2012. (Apr.).
Hassid, S., Santamouris, M., Papanikolaou, N., Linardi, A., Klitsikas, N., Georgakis, C., Assimakopoulos, D., 2000. The effect of the Athens heat island on air conditioning load. Energy Build. 32 (2), 131–141. https://doi.org/10.1016/s0378-7788(99)00045-6. (Jul.).
Hoffmann, P., Schlünzen, K.H., 2013. Weather pattern classification to represent the urban heat island in present and future climate. J. Appl. Meteorol. Climatol. 52 (12), 2699–2714. https://doi.org/10.1175/jamc-d-12-065.1. (Dec).
IPCC, 2013. Climate Change 2013: The Physical Science Basis. Contribution of Working Group I to the Fifth Assessment Report of the Intergovernmental Panel on Climate Change. Cambridge University Press, Cambridge, United Kingdom and New York, NY, USA. https://doi.org/10.1017/CBO9781107415324.
Isaac, M., Van Vuuren, D.P., 2009. Modeling global residential sector energy demand for heating and air conditioning in the context of climate change. Energy Policy 37 (2), 507–521. https://doi.org/10.1016/j.enpol.2008.09.051.
Jacob, D., Petersen, J., Eggert, B., Alias, A., Christensen, O.B., Bouwer, L.M., Braun, A., Colette, A., Déqué, M., Georgievski, G., Georgopoulou, E., Gobiet, A., Menut, L., Nikulin, G., Haensler, A., Hempelmann, N., Jones, C., Keuler, K., Kovats, S., Kröner, N., Kotlarski, S., Kriegsmann, A., Martin, E., van Meijgaard, E., Moseley, C., Pfeifer, S., Preuschmann, S., Radermacher, C., Radtke, K., Rechid, D., Rounsevell, M., Samuelsson, P., Somot, S., Soussana, J.-F., Teichmann, C., Valentini, R., Vautard, R., Weber, B., Yiou, P., 2013. EURO-CORDEX: new high-resolution climate change projections for european impact research. Reg. Environ. Chang. 14 (2), 563–578. https://doi.org/10.1007/s10113-013-0499-2. (Jul.).
Jandaghian, Z., Akbari, H., 2018. The effect of increasing surface albedo on urban climate and air quality: a detailed study for Sacramento, Houston, and Chicago. Climate 6 (2), 19. https://doi.org/10.3390/cli6020019. (Mar.).
Karl, T.R., Nicholls, N., Ghazi, A., 1999. CLIVAR/GCOS/WMO workshop on indices and indicators for climate extremes workshop summary. In: Weather and Climate Extremes. Springer, Netherlands, pp. 3–7. https://doi.org/10.1007/978-94-015-9265-9_2.
Krispel, S., Peyerl, M., Maier, G., Weihs, P., 2017. Urban Heat Islands - Reduktion von innerstädtischen Wärmeinseln durch Whitetopping. Bauphysik 39 (1), 33–40. https://doi.org/10.1002/bapi.201710002.
Landsberg, H.E., 1981. The Urban Climate. Elsevier Science, Stanford.
Laukkonen, J., Blanco, P.K., Lenhart, J., Keiner, M., Cavric, B., Kinuthia-Njenga, C., 2009. Combining climate change adaptation and mitigation measures at the local level. Habitat Int. 33 (3), 287–292. https://doi.org/10.1016/j.habitatint.2008.10.003. (Jul.).
Lauwaet, D., Hooyberghs, H., Maiheu, B., Lefebvre, W., Driesen, G., Looy, S.V., Ridder, K.D., 2015. Detailed urban heat island projections for cities worldwide: dynamical downscaling CMIP5 global climate models. Climate 3 (2), 391–415. https://doi.org/10.3390/cli3020391. (Jun.).
Lauwaet, D., Ridder, K.D., Saeed, S., Brisson, E., Chatterjee, F., van Lipzig, N., Maiheu, B., Hooyberghs, H., 2016. Assessing the current and future urban heat island of Brussels. Urban Clim. 15, 1–15. https://doi.org/10.1016/j.uclim.2015.11.008. (Mar.).
Lindberg, F., Holmer, B., Thorsson, S., Rayner, D., 2013. Characteristics of the mean radiant temperature in high latitude cities—implications for sensitive climate planning applications. Int. J. Biometeorol. 58 (5), 613–627. https://doi.org/10.1007/s00484-013-0638-y. (Feb.).
Lindberg, F., Thorsson, S., Rayner, D., Lau, K., 2016. The impact of urban planning strategies on heat stress in a climate-change perspective. Sustain. Cities Soc. 25, 1–12. https://doi.org/10.1016/j.scs.2016.04.004. (Aug).
McPherson, E.G., 1994. Cooling urban heat islands with sustainable landscapes. In: Platt, R.H., Rowntree, R., Muick, P.C. (Eds.), The Ecological City: Preserving and Restoring Urban Biodiversity. 151–171. University of Massachusetts Press, Amherst, MA, pp. 151–171.
Monteiro, M.V., Doick, K.J., Handley, P., Peace, A., 2016. The impact of greenspace size on the extent of local nocturnal air temperature cooling in London. Urban For. Urban Green. 16, 160–169. https://doi.org/10.1016/j.ufug.2016.02.008.
Moss, R.H., Edmonds, J.A., Hibbard, K.A., Manning, M.R., Rose, S.K., van Vuuren, D.P., Carter, T.R., Emori, S., Kainuma, M., Kram, T., Meehl, G.A., Mitchell, J.F.B., Nakicenovic, N., Riahi, K., Smith, S.J., Stouffer, R.J., Thomson, A.M., Weyant, J.P., Wilbanks, T.J., 2010. The next generation of scenarios for climate change research and assessment. Nature 463 (7282), 747–756. https://doi.org/10.1038/nature08823. (Feb.).
Müller, N., Kuttler, W., Barlag, A.-B., 2013. Counteracting urban climate change: adaptation measures and their effect on thermal comfort. Theor. Appl. Climatol. 115 (1–2), 243–257. https://doi.org/10.1007/s00704-013-0890-4. (Apr.).
Municipality of City of Klagenfurt, 2019a. Bevölkerungsentwicklung. Available from: https://www.klagenfurt.at/_Resources/Persistent/4cdbdeb20ffeecb5c86779053ced33629b34e77d/2019%20-%20Bev%C3%B6lkerung%202018%20-%20190411.pdf (Accessed 17 September 2019).
Municipality of City of Klagenfurt, 2019b. Klagenfurt am wörthersee. Available from: https://www.klagenfurt.at/die-stadt/statistik/bevoelkerung.html (Accessed 04 June 2019).
Oke, T.R., 1982. The energetic basis of the urban heat island. Q. J. R. Meteorol. Soc. 108 (455), 1–24. https://doi.org/10.1002/qj.49710845502. (Jan.).
Orehounig, K., Mahdavi, A., Doppelbauer, E.-M., Loibl, W., Tötzer, T., 2014. Projections of design implications on energy performance of future cities: a case study from Vienna. Sustain. Cities Soc. 12, 92–101. https://doi.org/10.1016/j.scs.2014.03.001. (Jul.).
Qiu, G.-Y., LI, H.-Y., Zhang, Q.-T., Wan, C., Liang, X.-J., Li, X.-Z., 2013. Effects of evapotranspiration on mitigation of urban temperature by vegetation and urban agriculture. J. Integr. Agric. 12 (8), 1307–1315. https://doi.org/10.1016/s2095-3119(13)60543-2. (Aug.).
Ridder, K.D., Lauwaet, D., Maiheu, B., 2015. UrbClim – a fast urban boundary layer climate model. Urban Clim. 12, 21–48. https://doi.org/10.1016/j.uclim.2015.01.001. (Jun.).
Santamouris, M., 2014. Cooling the cities – a review of reflective and green roof mitigation technologies to fight heat island and improve comfort in urban environments. Sol. Energy 103, 682–703. https://doi.org/10.1016/j.solener.2012.07.003. (May).
Santamouris, M., Synnefa, A., Karlessi, T., 2011. Using advanced cool materials in the urban built environment to mitigate heat islands and improve thermal comfort conditions. Sol. Energy 85 (12), 3085–3102. https://doi.org/10.1016/j.solener.2010.12.023. (Dec).
Senf, C., Pflugmacher, D., Zhiqiang, Y., Sebald, J., Knorn, J., Neumann, M., Hostert, P., Seidl, R., 2018. Canopy mortality has doubled in europe's temperate forests over the last three decades. Nat. Commun. 9https://doi.org/10.1038/s41467-018-07539-6. (Nov.).
Siebert, J., Sievers, U., Zdunkowski, W., 1992. A one-dimensional simulation of the interaction between land surface processes and the atmosphere. Bound.-Layer Meteorol. 59 (1–2), 1–34.
Sievers, U., 1995. Generalization of the streamfunction–vorticity method to three dimensions. Meteorol. Z. 3, 3–15.
Sievers, U., 2012. Das kleinskalige stromungsmodell muklimo_3 teil 1: Theoretische grundlagen, pc-basisversion und validierung. In: Berichte des Deutschen Wetterdienstes Band 240.
Sievers, U., 2016. Das kleinskalige stromungsmodell muklimo_3 teil 2: Thermodynamische erweiterungen. In: Berichte des Deutschen Wetterdienstes Band 248.
Sievers, U., Früh, B., 2012. A practical approach to compute short-wave irradiance interacting with subgrid-scale buildings. Meteorol. Z. 21 (4), 349–364.
Sievers, U., Zdunkowski, W., 1986. A microscale urban climate model. Contributions to Atmospharic Physics 59, 13–40.
Sievers, U., Forkel, R., Zdunkowski, W., 1983. Transport equations for heat and moisture in the soil and their application to boundary layer problems. Contrib. Atmos. Phys 56, 58–83.
Straka, M., Sodoudi, S., 2019. Evaluating climate change adaptation strategies and scenarios of enhanced vertical and horizontal compactness at urban scale (a case study for berlin). Landsc. Urban Plan. 183, 68–78. https://doi.org/10.1016/j.landurbplan.2018.11.006. (Mar.).
Synnefa, A., Dandou, A., Santamouris, M., Tombrou, M., Soulakellis, N., 2008. On the use of cool materials as a heat island mitigation strategy. J. Appl. Meteorol. Climatol. 47 (11), 2846–2856. https://doi.org/10.1175/2008jamc1830.1. (Nov.).

Taha, H., 1997. Urban climates and heat islands: albedo, evapotranspiration, and anthropogenic heat. Energy Build. 25 (2), 99–103. https://doi.org/10.1016/s0378-7788(96)00999-1. (Jan).
Taha, H., Akbari, H., Rosenfeld, A., Huang, J., 1988. Residential cooling loads and the urban heat island—the effects of albedo. Build. Environ. 23 (4), 271–283. https://doi.org/10.1016/0360-1323(88)90033-9. (Jan.).
Taleghani, M., 2018. The impact of increasing urban surface albedo on outdoor summer thermal comfort within a university campus. Urban Clim. 24, 175–184. https://doi.org/10.1016/j.uclim.2018.03.001.
Townsend-Small, A., Czimczik, C.I., 2010. Carbon sequestration and greenhouse gas emissions in urban turf. Geophys. Res. Lett. 37 (2). https://doi.org/10.1029/2009gl041675. n/a–n/a. (Jan.).
UN, 2018. World Urbanization Prospects. United NationsAvailable from. https://population.un.org/wup/Publications/Files/WUP2018-KeyFacts.pdf (Accessed 21 May 2019).
UN, 2019. Sustainable Development Goals. United NationsAvailable from. https://www.un.org/sustainabledevelopment/cities/.
van Ruijven, B.J., De Cian, E., Wing, I.S., 2019. Amplification of future energy demand growth due to climate change. Nat. Commun. 10 (1), 2762. https://doi.org/10.1038/s41467-019-10399-3.
Voskamp, I., de Ven, F.V., 2015. Planning support system for climate adaptation: composing effective sets of blue-green measures to reduce urban vulnerability to extreme weather events. Build. Environ. 83, 159–167. https://doi.org/10.1016/j.buildenv.2014.07.018. (Jan.).
WCRP, 2019. World Climate Research ProgrammeAvailable from. http://www.cordex.org/ (Accessed 07 May 2019).
Willmott, C., Ackleson, S., Davis, R., Feddema, J., Klink, K., Legates, D., O'donnell, J., Rowe, C., 1985. Statistics for the evaluation of model performance. J. Geophys. Res. 90 (C5), 8995–9005.
ZAMG, 2019. Meteorological measurements, data set from 1767 to 2018. In: Central Institution for Meteorology and Geodynamics (ZAMG).
Zhang, G., He, B.-J., Zhu, Z., Dewancker, B.J., 2019. Impact of morphological characteristics of green roofs on pedestrian cooling in subtropical climates. Int. J. Environ. Res. Public Health 16 (2), 179. https://doi.org/10.3390/ijerph16020179. (Jan.).
Zhou, B., Rybski, D., Kropp, J.P., 2017. The role of city size and urban form in the surface urban heat island. Sci. Rep. 7https://doi.org/10.1038/s41598-017-04242-2. (Jul.).
Žuvela-Aloise, M., Koch, R., Neureiter, A., Bohm, R., Buchholz, S., 2014. Reconstructing urban climate of vienna based on historical maps dating to the early instrumental period. Urban Climat. 10, 490–508. https://doi.org/10.1016/j.uclim.2014.04.002.
Žuvela-Aloise, M., Andre, K., Schwaiger, H., Bird, D.N., Gallaun, H., 2017. Modelling reduction of urban heat load in Vienna by modifying surface properties of roofs. Theor. Appl. Climatol. 131, 1005–1018. https://doi.org/10.1007/s00704-016-2024-2.